3638 *Chem. Mater.* **2009,** *21,* 3638–3648
DOI:10.1021/cm901025n

CHEMISTRY OF MATERIALS
Article

Peptide Brush—Ordered Mesoporous Silica Nanocomposite Materials

Jonathan D. Lunn and Daniel F. Shantz*

Artie McFerrin Department of Chemical Engineering, Texas A&M University, 3122 TAMU, College Station, Texas 77843-3122

Received April 14, 2009. Revised Manuscript Received June 17, 2009

Organic−inorganic nanocomposites are synthesized through the surface-initiated polymerization of *N*-carboxyanhydrides from amine-functionalized ordered mesoporous silica (OMS). Composites with high densities of grafted peptide were obtained which possess dramatically decreased porosity compared to the parent OMS material. The effect of the amine loading, pore size, pore topology, and monomer identity on the peptide brush layer obtained is investigated. Nitrogen porosimetry, thermal gravimetric analysis, elemental analysis, infrared and NMR spectroscopy, and mass spectrometry verify the formation of the peptide brushes and indicate much of the organic phase formed is in the silica mesopores. The L-Lys(Z) peptide brushes can be deprotected on the solid surface as evidenced by thermal gravimetric analysis, infrared spectroscopy, and NMR spectroscopy. L-Ala peptide brushes may also be synthesized, and polymer growth confinement is evidenced by mass spectrometry as the number of alanine units per brush appears dependent on the silica pore size/topology.

Introduction

The ability to tune and construct well-defined organic−inorganic hybrids for applications such as catalysis, separations, and sensing has been a major goal of many researchers over the last few decades.[1−6] Of particular interest to the current work are ceramics decorated with organic layers, as the ceramic support provides mechanical and thermal stability while the organic layer adds specific chemical functionality. Ordered mesoporous silicas (OMS) are especially useful inorganic supports for scientific investigation due to their controllable pore size (2−15 nm), ease of functionalization through silane chemistry, and ordered/uniform pore network that facilitates analysis by standard techniques such as powder X-ray diffraction (PXRD), electron microscopy, and porosimetry.[7−13]

Numerous groups have investigated the incorporation of small organic functional groups into OMS through covalent and noncovalent approaches.[2,14−20] Covalent functionalization, typically through silane chemistry, has been accomplished through both direct (co-condensation) and indirect (postsynthetic grafting) methods.[21] More recently, larger chemical moieties have been incorporated into OMS, including organometallic catalysts,[1,22] dendrimers,[23−25] and enzymes[22] by further functionalization of smaller functional groups, such as amines, thiols, alkyl halides, and alkenes. There has also been significant development in the area of periodic mesoporous organosilicas synthesized by the self-assembly of bisilylated organic monomers.[26]

*Corresponding author. Phone: (979) 845-3492. Fax: (979) 845-6446. E-mail: shantz@chemail.tamu.edu.

(1) Ford, D. M.; Simanek, E. E.; Shantz, D. F. *Nanotechnology* **2005**, *16*, S458–S475.
(2) Moller, K.; Bein, T. *Chem. Mater.* **1998**, *10*, 2950–2963.
(3) Hoffmann, F.; Cornelius, M.; Morell, J.; Froba, M. *Angew. Chem., Int. Ed.* **2006**, *45*, 3216–3251.
(4) Sanchez, C.; Julian, B.; Belleville, P.; Popall, M. *J. Mater. Chem.* **2005**, *15*, 3559–3592.
(5) Sanchez, C.; Soler-Illia, G.; Ribot, F.; Lalot, T.; Mayer, C. R.; Cabuil, V. *Chem. Mater.* **2001**, *13*, 3061–3083.
(6) Stein, A.; Melde, B. J.; Schroden, R. C. *Adv. Mater.* **2000**, *12*, 1403–1419.
(7) Beck, J. S.; Vartuli, J. C.; Roth, W. J.; Leonowicz, M. E.; Kresge, C. T.; Schmitt, K. D.; Chu, C. T. W.; Olson, D. H.; Sheppard, E. W.; McCullen, S. B.; Higgins, J. B.; Schlenker, J. L. *J. Am. Chem. Soc.* **1992**, *114*, 10834–10843.
(8) Davis, M. E. *Nature* **2002**, *417*, 813–821.
(9) Edler, K. J.; White, J. W. *Chem. Mater.* **1997**, *9*, 1226–1233.
(10) Kleitz, F.; Choi, S. H.; Ryoo, R. *Chem. Commun.* **2003**, *17*, 2136–2137.
(11) Stein, A. *Adv. Mater.* **2003**, *15*, 763–775.
(12) Zhao, D. Y.; Huo, Q. S.; Feng, J. L.; Chmelka, B. F.; Stucky, G. D. *J. Am. Chem. Soc.* **1998**, *120*, 6024–6036.
(13) Kresge, C. T.; Leonowicz, M. E.; Roth, W. J.; Vartuli, J. C.; Beck, J. S. *Nature* **1992**, *359*, 710–712.
(14) Bass, J. D.; Anderson, S. L.; Katz, A. *Angew. Chem., Int. Ed.* **2003**, *42*, 5219–5222.
(15) Bass, J. D.; Katz, A. *Chem. Mater.* **2003**, *15*, 2757–2763.
(16) Bass, J. D.; Katz, A. *Chem. Mater.* **2006**, *18*, 1611–1620.
(17) Lim, M. H.; Blanford, C. F.; Stein, A. *J. Am. Chem. Soc.* **1997**, *119*, 4090–4091.
(18) McKittrick, M. W.; Jones, C. W. *Chem. Mater.* **2003**, *15*, 1132–1139.
(19) McKittrick, M. W.; Jones, C. W. *J. Am. Chem. Soc.* **2004**, *126*, 3052–3053.
(20) Hicks, J. C.; Jones, C. W. *Langmuir* **2006**, *22*, 2676–2681.
(21) Lim, M. H.; Stein, A. *Chem. Mater.* **1999**, *11*, 3285–3295.
(22) Zhao, X. S.; Bao, X. Y.; Guo, W. P.; Lee, F. Y. *Mater. Today* **2006**, *9*, 32–39.
(23) Acosta, E. J.; Carr, C. S.; Simanek, E. E.; Shantz, D. F. *Adv. Mater.* **2004**, *16*, 985–989.
(24) Reynhardt, J. P. K.; Yang, Y.; Sayari, A.; Alper, H. *Adv. Funct. Mater.* **2005**, *15*, 1641–1646.
(25) Yoo, S.; Lunn, J. D.; Gonzalez, S.; Ristich, J. A.; Simanek, E. E.; Shantz, D. F. *Chem. Mater.* **2006**, *18*, 2935–2942.
(26) Fujita, S.; Inagaki, S. *Chem. Mater.* **2008**, *20*, 891–908.

Published on Web 07/15/2009

Since the discovery of *N*-carboxyanhydrides (NCAs) by Hermann Leuchs in 1906,[27−29] NCAs have been used to synthesize a diverse set of materials from stepwise constructed peptides[30] to drug-delivery devices[31,32] and polymeric brushes[33] and as templates for inorganic oxides.[34−37] As polypeptides are responsive to external stimuli (pH, electrolytes, solvent, and temperature) and offer a wide range of side chain chemistries (thiols, amines, carboxylic acids, etc.), they are very suitable organic components in hybrid materials for possible applications such as chiral separations, solid asymmetric catalysts, drug delivery, and sensing. As such, there has been significant interest recently in grafting polypeptides to inorganic surfaces, primarily to silicon or quartz planar surfaces,[38−45] though there have also been studies on gold supported SAMS[46,47] and colloidal silica.[48,49] There have also been several investigations of polypeptides grafted onto silica/alumina as chiral stationary phases[50,51] and on colloidal silica crystals for use as membranes.[52] However, to our knowledge, there have been no reported works of polypeptide grafting to OMS through NCA chemistry.

Many reports investigating other polymers in OMS, predominantly through radical polymerization, however, can be found in the literature. For example, atom transfer radical polymerization (ATRP) has been used by Kruk et al. to graft polyacrylonitrile, poly(2-(dimethylamino)ethyl methacrylate), and polystyrene to FDU-1 and SBA-15.[53] Audioun et al.[54] and Moreno et al.[55] similarly reported polymerizations using methyl methacrylate (MMA) and its derivatives in SBA-15 by ATRP. Polymers have also been incorporated into MCM-41 by radical polymerizations: Lenarda et al. used nitroxide-mediated polymerization (NMP) to graft polystyrene,[56] and Moller et al.[57a] performed a free radical polymerization to graft PMMA. Free radical polymerization has also been used to incorporate polystyrene in the cubic MCM-48 by He et al.[57b] Polymers "threaded" through the pores of OMS, such as the conductive polyaniline, have also been reported.[58−61] Additionally, there have been studies functionalizing OMS with polyethyleneimine (PEI) through the ring-opening polymerization of aziridine.[62−64]

Herein, we report the grafting of poly-Z-L-lysine (PZK) and poly-L-alanine (PA) in the OMS materials MCM-41, SBA-15, and KIT-6. The effects of pore size, pore topology, surface initiator loading, and monomer identity are discussed on the basis of the characterization of these materials by a battery of methods, including porosimetry, thermogravimetric analysis, infrared spectroscopy, X-ray photoelectron spectroscopy, solid-state NMR, and mass spectrometry.

Experimental Section

Materials. Sodium silicate (PQ Brand N, SiO_2 28.7%, $SiO_2/Na_2O = 3.22$), cetyltrimethylammonium bromide (CTAB, Fisher Chemical, high purity grade), H_2SO_4 (Sigma-Aldrich, 95−98% ACS reagent), sodium hydroxide (NaOH, Mallinckrodt Chemicals, pellet), tetraethoxysilane (TEOS, Fluka, >99%), Pluronic P123 ($EO_{20}PO_{70}EO_{20}$, MW = 5800, BASF), ethanol (Sigma-Aldrich, 99.9%, ACS reagent), *n*-butanol (EMD, 99%), and HCl (Sigma-Aldrich, reagent grade, 37%) were used in the OMS syntheses as received. 3-Aminopropyltrimethoxysilane (APTMS, Aldrich, 97%) was used for postsynthetic grafting and distilled prior to use. Triphosgene (TCI America, 98%), H-Lys(Z)-OH (Novabiochem, 98%), and L-alanine (Aldrich, 99%) were used for *N*-carboxyanhydride syntheses. *n*-Hexane (Sigma-Aldrich, >95%, ACS reagent grade), tetrahydrofuran (THF, Sigma-Aldrich, >99.9%, Chromasolv HPLC), and toluene (Sigma-Aldrich >99.5%, ACS reagent grade) were used in the postsynthetic grafting, NCA synthesis, and polymer grafting steps and were dried and deoxygenated using an MBRAUN MB SPS solvent purification system. Nitromethane (ACROS, 98%), nitrobenzaldehyde (Fluka, >99%, HPLC), and deuterated chloroform (Cambridge

(27) Leuchs, H. *Berichte Der Deutschen Chemischen Gesellschaft* **1906**, *39*, 857–861.
(28) Leuchs, H.; Felser, H. *Berichte Der Deutschen Chemischen Gesellschaft* **1908**, *41*, 1726–1735.
(29) Leuchs, H.; Manasse, W. *Berichte Der Deutschen Chemischen Gesellschaft* **1907**, *40*, 3235–3249.
(30) Sim, T. B.; Rapoport, H. *J. Org. Chem.* **1999**, *64*, 2532–2536.
(31) Kataoka, K.; Kwon, G. S.; Yokoyama, M.; Okano, T.; Sakurai, Y. *J. Controlled Release* **1993**, *24*, 119–132.
(32) Nakanishi, T.; Fukushima, S.; Okamoto, K.; Suzuki, M.; Matsumura, Y.; Yokoyama, M.; Okano, T.; Sakurai, Y.; Kataoka, K. *J. Controlled Release* **2001**, *74*, 295–302.
(33) Takaki, M.; Asam, R.; Hanada, Y.; Ochiai, N. *Polym. Bull.* **1987**, *18*, 105–110.
(34) Hawkins, K. M.; Wang, S. S. S.; Ford, D. M.; Shantz, D. F. *J. Am. Chem. Soc.* **2004**, *126*, 9112–9119.
(35) Jan, J. S.; Lee, S. J.; Carr, C. S.; Shantz, D. F. *Chem. Mater.* **2005**, *17*, 4310–4317.
(36) Jan, J. S.; Shantz, D. F. *Chem. Commun.* **2005**, 2137–2139.
(37) Jan, J. S.; Shantz, D. F. *Adv. Mater.* **2007**, *19*, 2951–+.
(38) Chang, Y.-C.; Frank, C. W. *Langmuir* **1996**, *12*, 5824–5829.
(39) Chang, Y.-C.; Frank, C. W. *Langmuir* **1998**, *14*, 326–334.
(40) Heise, A.; Menzel, H.; Yim, H.; Foster, M. D.; Wieringa, R. H.; Schouten, A. J.; Erb, V.; Stamm, M. *Langmuir* **1997**, *13*, 723–728.
(41) Wang, Y.; Chang, Y.-C. *Macromolecules* **2003**, *36*, 6503–6510.
(42) Wang, Y.; Chang, Y.-C. *Macromolecules* **2003**, *36*, 6511–6518.
(43) Wang, Y.; Chang, Y.-C. *Adv. Mater.* **2003**, *15*, 290–293.
(44) Wieringa, R. H.; Siesling, E. A.; Geruts, P. F. M.; Werkman, P. J.; Vorenkamp, E. J.; Erb, V.; Stamm, M.; Schouten, A. J. *Langmuir* **2001**, *17*, 6477–6484.
(45) Wieringa, R. H.; Siesling, E. A.; Geruts, P. F. M.; Werkman, P. J.; Vorenkamp, E. J.; Erb, V.; Stamm, M.; Schouten, A. J. *Langmuir* **2001**, *17*, 6485–6490.
(46) Jaworek, T.; Neher, D.; Wegner, G.; Wieringa, R. H.; Schouten, A. J. *Science* **1998**, *279*, 57–60.
(47) Whitesell, J. K.; Chang, H. K. *Science* **1993**, *261*, 73–76.
(48) Fong, B.; Russo, P. S. *Langmuir* **1999**, *15*, 4421–4426.
(49) Fong, B.; Turksen, S.; Russo, P. S.; Stryjewski, W. *Langmuir* **2004**, *20*, 266–269.
(50) Czaun, M.; Rahman, M. M.; Takafuji, M.; Ihara, H. *Polymer* **2008**, *49*, 5410–5416.
(51) Shundo, A.; Sakurai, T.; Takafuji, M.; Nagaoka, S.; Ihara, H. *J. Chromatogr., A* **2005**, *1073*, 169–174.
(52) Abelow, A. E.; Zharov, I. *Soft Matter* **2009**, *5*, 457–462.
(53) Kruk, M.; Dufour, B.; Celer, E. B.; Kowalewski, T.; Jaroniec, M.; Matyjaszewski, K. *Macromolecules* **2008**, *41*, 8584–8591.
(54) Audouin, F.; Blas, H.; Pasetto, P.; Beaunier, P.; Boissiere, C.; Sanchez, C.; Save, M.; Charleux, B. *Macromol. Rapid Commun.* **2008**, *29*, 914–921.
(55) Moreno, J.; Sherrington, D. C. *Chem. Mater.* **2008**, *20*, 4468–4474.
(56) Lenarda, M.; Chessa, G.; Moretti, E.; Polizzi, S.; Storaro, L.; Talon, A. *J. Mater. Sci.* **2006**, *41*, 6305–6312.
(57) (a) Moller, K.; Bein, T.; Fischer, R. X. *Chem. Mater.* **1999**, *11*, 665–673. (b) He, J.; Shen, Y.; Evans, D. G. *Microporous Mesoporous Mater.* **2008**, *109*, 73–83.
(58) Frisch, H. L.; Mark, J. E. *Chem. Mater.* **1996**, *8*, 1735–1738.
(59) Wu, C. G.; Bein, T. *Science* **1994**, *266*, 1013–1015.
(60) Wu, C. G.; Bein, T. *Chem. Mater.* **1994**, *6*, 1109–1112.
(61) Wu, C. G.; Bein, T. *Science* **1994**, *264*, 1757–1759.
(62) Hicks, J. C.; Drese, J. H.; Fauth, D. J.; Gray, M. L.; Qi, G. G.; Jones, C. W. *J. Am. Chem. Soc.* **2008**, *130*, 2902–2903.
(63) Rosenholm, J. M.; Duchanoy, A.; Linden, M. *Chem. Mater.* **2008**, *20*, 1126–1133.
(64) Rosenholm, J. M.; Penninkangas, A.; Linden, M. *Chem. Commun.* **2006**, 3909–3911.

Isotope, 99.8% D, 1% v/v TMS) were used as received for the Henry reaction. Hydrofluoric acid (Sigma-Aldrich, 48 wt % in water) and 1,1,1,3,3,3-hexafluoroisopropanol (Aldrich, >99%) were used in the silica framework dissolution. ***CAUTION****: Hydrofluoric acid is extremely toxic and should only be used following strict safety protocols.*

Synthesis of MCM-41, SBA-15, and KIT-6. MCM-41 was synthesized using the reported procedure of Edler and White.[9] A total of 7.9 g of sodium silicate solution were mixed with 45.4 mL of deionized water. A total of 0.27 g of NaOH were added to the solution, and then 7.8 mL of 1 M H_2SO_4 were added. A total of 7.29 g of CTAB were dissolved in the solution and stirred for 15 min at room temperature. The mixture was then placed in an oven at 100 °C for 24 h under static conditions. After 24 h the sample was removed from the oven and allowed to cool sufficiently that it could be easily handled and titrated to a pH of approximately 10 using 1 M H_2SO_4. The sample was then placed back in the oven at 100 °C. The titration step was performed two additional times at regular 24 h intervals. The total heating period was 96 h. The solid products were filtered, washed with deionized water, and air-dried overnight. The solid products were calcined to remove CTAB. The calcination procedure was as follows: the air-dried samples were heated from room temperature to 100 °C at a rate of 1 °C/min; held at 100 °C for 2 h; increased from 100 to 500 °C at a rate of 1 °C/min; and then held at 500 °C for 5 h.

SBA-15 samples were synthesized using the method reported by Zhao and co-workers.[12] A total of 4.0 g of Pluronic P123 were dissolved in 60 mL of 4 M HCl and 85 mL of deionized water by stirring for 5 h at room temperature. Then, 8.5 g of TEOS were added to that solution and stirred for 24 h at 35 °C. The mixture was then aged at 80 °C for 24 h without stirring. After filtering, the solid product was calcined for 5 h at 550 °C in a similar manner to the MCM-41 procedure described above.

KIT-6 was synthesized according to the method reported by Kleitz et al.[10] A total of 6 g of Pluronic P123 were dissolved in 217 g of DI water and 11.8 g of concentrated HCl (35%). After warming to 35 °C and while stirring, 6 g of butanol were added. After 1 h of stirring, 12.9 g of TEOS were added, and the mixture was subsequently stirred at 35 °C for 24 h. Immediately following, the mixture was heated to 100 °C for an additional 24 h under static conditions. The solid product was filtered while still hot, and the Pluronic was removed by extraction in a mixture of HCl and ethanol. After drying at room temperature, the solid product was calcined at 500 °C.

Amine Functionalization of MCM-41, SBA-15 ,and KIT-6. Amine-functionalized OMS was prepared using postsynthetic grafting. All reagents and OMS were handled under an inert atmosphere. In a typical grafting, one gram of OMS was heated and dried under vacuum overnight (<0.1 mbar, ~100 °C). A total of 50 mL of dry toluene were added, followed by 0.25 mmol, 0.5 mmol, or 0.75 mmol of distilled APTMS depending upon the desired degree of functionalization. The reaction proceeded at RT for 24 h. The solid product was centrifuged, washed in toluene (1×), methanol (1×), methanol/water (1×), and methanol (1×) and dried overnight in a 40 °C oven.

***N*-Carboxyanhydride Synthesis.** The N_ε-Z-L-Lysine (L-Lys(Z)) NCA was synthesized in dry THF using triphosgene as described by Daly and Poche[65] (Scheme 1). Standard Schlenk line techniques were employed in the NCA monomer synthesis and polymer grafting steps. Typically, 4.6 g of L-Lys(Z)

(65) Daly, W. H.; Poche, D. *Tetrahedron Lett.* **1988**, *29*, 5859–5862.

Scheme 1. *N*-Carboxyanhydride Synthesis[a]

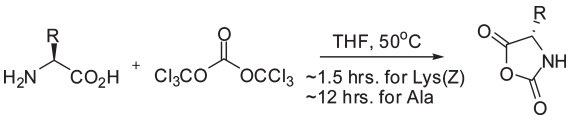

[a] R = $-CH_3$ for L-Ala and $-CH_2CH_2CH_2CH_2NHCbz$ for L-Lys(Z).

Scheme 2. Schematic of Peptide Grafting to Silica Surface[a]

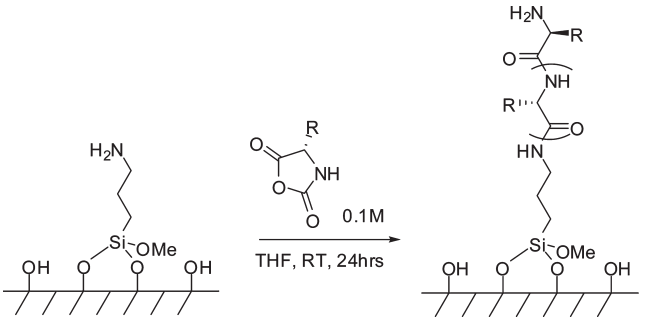

[a] R = $-CH_3$ for L-Ala and $-CH_2CH_2CH_2CH_2NHCbz$ for L-Lys(Z).

(16.4 mmol) and 2.2 g of triphosgene (7.4 mmol) were dried under vacuum for a minimum of 20 min in separate Schlenk flasks. A total of 75 and 50 mL of dry THF were added to the L-Lys(Z) and triphosgene, respectively, directly from the solvent drying system. The triphosgene solution was added via cannula transfer to a rapidly mixing L-Lys(Z) slurry. The reaction flask was capped and placed in a 50 °C water bath. After ~1.5 h of stirring at 50 °C under argon, the solution became transparent, indicating the completion of the reaction. The NCA was recrystallized in 400 mL of dry *n*-hexane overnight in a standard freezer twice and, subsequently, filtered and dried under vacuum for immediate use (~5 g or >95% yield). L-Alanine NCA was prepared in a similar fashion with two notable differences: 8.1 mmol of triphosgene and NCA synthesis took place overnight. The yield of L-Ala NCA was 64%.

Polymerization. The NCA was polymerized in a *graft from* approach using the amines on the OMS surface as initiators (Scheme 2). In a typical procedure, 0.5 g of amine-functionalized OMS were heated and dried overnight under vacuum. A 0.1 M NCA solution was prepared in dry THF, and 50 mL were transferred to the dried OMS via cannula (40:1 monomer/initiator for the 0.25 mmol APTMS/g SiO_2, 20:1 and 13:1 for the 0.5 and 0.75 mmol APTMS/g SiO_2 substrates, respectively). The powder and solution were vigorously stirred at room temperature for 24 h. After completion, the powder was centrifuged and rinsed in 50 mL of THF (2×), DMF (2×), and chloroform (2×). The composite was dried in a 40 °C oven and stored.

Deprotection. The Cbz-protected peptides were deprotected using a 33 wt % solution of HBr in acetic acid. For example, 200 mg of composite material were stirred for 30 min in 2 mL of HBr solution. The composite was filtered and rinsed multiple times with toluene and acetone. The sample was neutralized by stirring in a 1 mM NaOH solution overnight and then filtered and rinsed with water and methanol.

Catalytic Testing. The nitroaldol reaction (Henry reaction) was used to test the catalytic activity of the peptide−OMS composites in the manner performed by Bass and co-workers.[14] For each test, 0.38 g of 4-nitrobenzaldehyde (2.5 mmol) were added to a 10 mL Schlenk flask with 10−25 mg of predried deprotected peptide−OMS composite (0.025 mmol on amine basis; calculated from TGA results). The composite and

4-nitrobenzaldehyde were dried under vacuum for 1 h, followed by the addition of 1.35 mL of nitromethane (25 mmol). The mixture was stirred at 40 °C under argon for 7 h. Aliquots of 50 μL were removed every 30 min for the first 2 h and then again at 7 h. The aliquots were analyzed by ^{1}H NMR in *d*-chloroform. The conversion and yields were calculated by integrating the peaks for the β-hydroxyl (^{1}H δ 5.6 ppm) and α,β-unsaturated (^{1}H δ 7.72−7.75 ppm) products with respect to that of 4-nitrobenzaldehyde (^{1}H δ 10.1 ppm).

Analytical Details. Powder X-ray diffraction (PXRD) measurements on MCM-41 were performed using a Bruker-AXS D8 powder diffractometer with Cu Kα radiation. X-ray diffraction measurements were performed on SBA-15 and KIT-6 samples using a Bruker-AXS Rotating-Anode NANO-STAR small angle X-ray scattering instrument with Cu Kα radiation. Infrared spectroscopy was performed on the composites using a Nexus 670 FT-IR spectrometer from Thermo Nicolet. Thermal gravimetric analyses (TGA) were performed using a TG 209C Iris Instrument from Netzsch over a temperature range of 100 to 550 °C using oxygen and nitrogen purges (1:1, 10 mL/min) and a temperature ramping rate of 1 °C min^{-1}. Nitrogen adsorption experiments were performed on a Micromeritics ASAP 2010 micropore system. The samples were degassed under vacuum at 100 °C overnight prior to analysis. The surface areas and mesopore volumes were determined using the α_s-method. The mesopore size distributions were calculated from the adsorption branch of the isotherm using the Barret-Joyner-Halenda (BJH) method. ^{13}C{^{1}H} CP-MAS analyses were performed at 100.61 MHz using a 4 mm probe with ZrO_2 rotors and a spinning rate of 9 kHz, a 2 ms contact time, a ^{1}H 90° pulse length of 2.5 μs, and a 5 s recycle delay. Chemical shifts were referenced to tetramethylsilane. X-ray photoelectron spectroscopy (XPS) was performed on a Kratos Axis Ultra Imaging XPS using a monochromatic Al Kα source. Solution ^{1}H NMR spectra were measured on a 300 MHz Varian Mercury spectrometer. The ^{1}H 90° pulse length was 6 μs, the recycle delay was 6 s, and 16 FIDs were recorded per spectrum. Chemical shifts were reference to TMS. Mass spectra were acquired using matrix-assisted laser desorption/ionization time-of-flight (MALDI-TOF) on an Applied Biosystems Voyager-DE STR Biospectrometry Workstation. Positive ion mode and a 2,4,6-trihydroxyacetophenone (THAP) matrix were used. Samples were prepared for MALDI-TOF MS by dissolving approximately 20 mg of composite in 2 mL of a 1:1 solution of 48 wt % aqueous HF and 1,1,1,3,3,3-hexafluoroisopropanol. Elemental analysis was performed by Galbraith laboratories.

Results

Parent Materials. The parent materials were characterized by porosimetry and PXRD to confirm synthesis of the desired mesophase and accurately determine the effect of peptide grafting. Figure 1 shows representative PXRD results for the parent OMS materials, and Figure 2 shows their nitrogen adsorption isotherms. For MCM-41, the (100), (110);, and (210) reflections can be clearly seen in the PXRD pattern; though much more subtle, the (210) is also present at 6° 2θ. The characteristic (100), (110), and (200) reflections are also observed for SBA-15 confirming the hexagonal pore arrangement. In the KIT-6 cubic pattern, the (211) peak at approximately 0.9° 2θ dwarfs the neighboring (220) reflection. Two broad peaks are also present between 1.4° 2θ and 2.0° 2θ which encompass the (321), (400), (420), (322), (422), and (431) reflections.

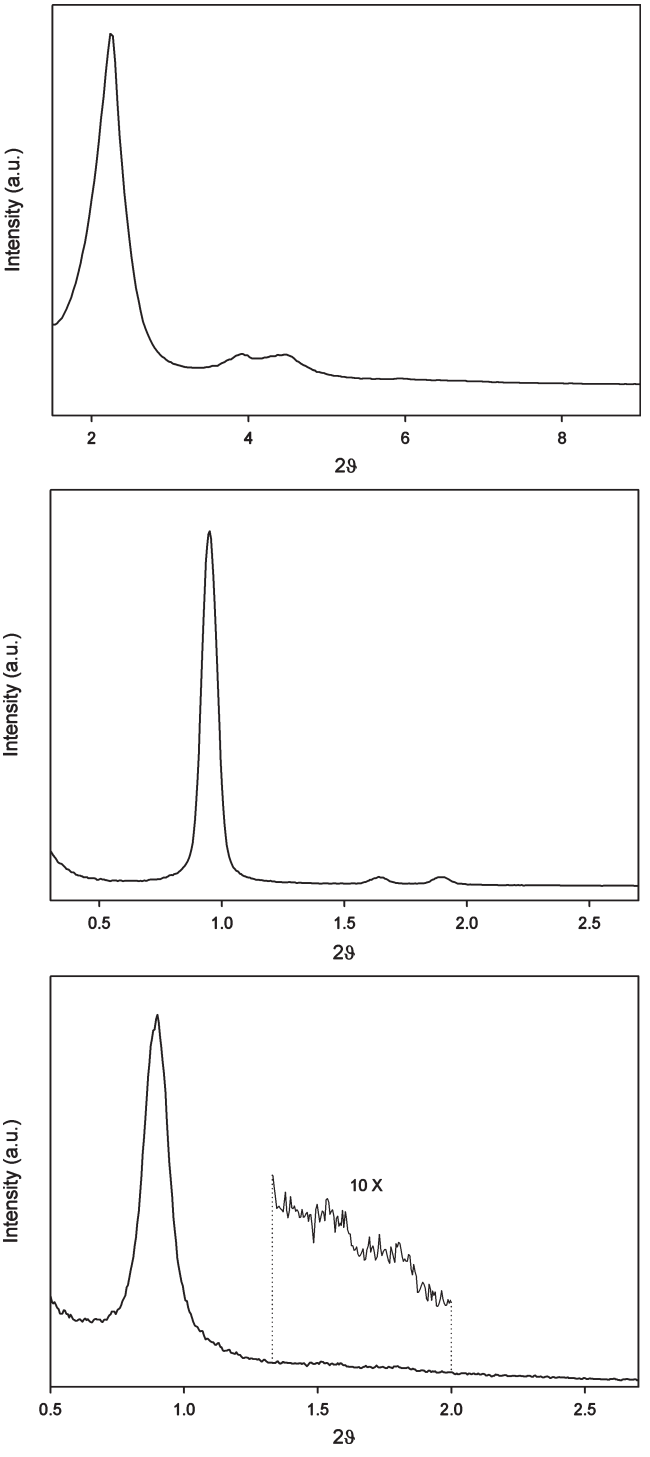

Figure 1. PXRD of MCM-41 (top); SBA-15 (middle); and KIT-6 (bottom).

The adsorption isotherms of each substrate are also indicative of successful mesophase synthesis. A summary of the findings from nitrogen adsorption is given in Tables 1 and 4, along with the composite adsorption data.

Poly-Z-L-lysine (PZK)−OMS Composites. *N_2 Adsorption.* Nitrogen adsorption was used to quantify the changes in porosity in the OMS resulting from peptide grafting. The α_s and BJH methods were used to calculate the surface area, pore volume, and pore size distribution. These results are summarized in Table 1. In both the

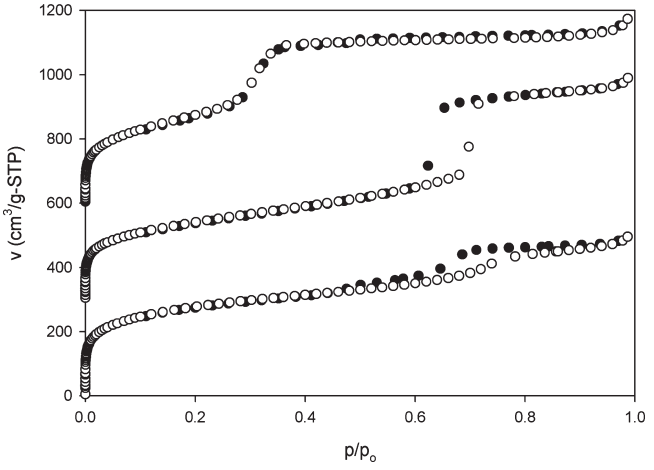

Figure 2. Adsorption isotherms of MCM-41 (top); SBA-15 (middle); and KIT-6 (bottom). The adsorption branch is represented by open circles; desorption by closed circles. The offset between isotherms is 300 cm^3/g-STP.

Table 1. Tabulated Nitrogen Adsorption Results for the Poly-Z-L-lysine–OMS Composites

sample ID	$S(\alpha_s)$ [m^2/g]	V_{meso} [cm^3/g]	d_p(BJH) [nm]
MCM-41	1083	0.72	2.8
PZK-0.25APTMS-MCM41	367	0.17	2.3
PZK-0.50APTMS-MCM41	70	~0	
PZK-0.75APTMS-MCM41	38	~0	
SBA-15	918	0.93	7.0
PZK-0.25APTMS-SBA15	102	0.06	6.3
PZK-0.50APTMS-SBA15	22	~0	
PZK-0.75APTMS-SBA15	10	~0	
KIT-6	1065	0.62	7.6
PZK-0.50APTMS-KIT6	309	0.11	6.8
PZK-0.25APTMS-KIT6	591	0.25	6.6
PZK-0.75APTMS-KIT6	105	0.07	5.9

MCM-41 and SBA-15 composites of PZK the pore volumes and surface areas drop dramatically after polymerization. Note that previous work from our lab[23,25] and others has shown that amine functionalization results in only very small (< 10%) changes in the nominal pore size and pore volume. Control experiments (not shown) indicate that the silanol groups of the OMS surface do not act as initiators for the ring-opening polymerization. The low initiator loading samples maintain some porosity, while the two higher loadings exhibit little or none. The KIT-6 composites behave quite differently, despite the similar pore size and surface area of the parent material as compared to SBA-15; the pore volume, surface area, and pore diameter decrease steadily with increasing initiator loading. Some porosity and surface area is maintained even at the highest initiator loading. The explanation for this is likely related to the difference in pore topology/surface characteristics of KIT-6.

Thermogravimetric Analysis. TGA was performed on the composite materials to determine the degree of organic functionalization. The MCM-41 based composites had weight losses of 41.8 wt %, 42.3 wt %, and 31.2 wt % for the 0.75, 0.50, and 0.25 mmol APTMS/g MCM-41 peptide composites, respectively. The SBA-15 composites showed slightly higher organic contents: 49.3 wt %, 47.3 wt %, and 30.3 wt % for the 0.75, 0.50, and 0.25 mmol APTMS/g SBA-15 peptide composites, respectively. The KIT-6 composites showed a much lower degree of functionalization with 31.6 wt %, 16.2 wt %, and 9.6 wt % for 0.75, 0.50, and 0.25 mmol/g initial amine loadings, respectively.

The highest two initial amine loadings for MCM-41 have high and essentially equal organic contents. This result is consistent with the adsorption data that show no porosity in these samples. It also provides substantial evidence that the pores are not merely blocked but completely filled with organic material. This same conclusion is true for the highest two initial amine loadings for SBA-15, except the organic content is about 15% higher due to the increased pore volume (by 29%). The 0.25 mmol APTMS/g SiO_2 composites for MCM-41 and SBA-15 show about a quarter reduction in their organic content compared to the higher initiator loadings. This result is again consistent with the porosimetry results that show larger mesopore volumes in these two samples with respect to the samples with higher initial amine loadings. With regards to the KIT-6 composites, TGA shows that there is much less organic grafted than might be expected based on the other OMS composites. Just as in the other OMS composites, the TGA data matches very nicely with the adsorption isotherms: less organic leads to more porosity. The results for the KIT-6 composites seem to indicate the ability to tune the porosity and organic content by changing the initiator loading.

Elemental Analysis. Elemental analysis was performed to verify our TGA results/calculations, as well as the spectroscopic methods that show peptide is formed in the composite. C/N ratios (on a molar basis) and C/Si (on a weight basis) from our TGA calculations (and XPS for C/N, vide infra) are compared with those from elemental analysis (Table 2). Complete EA results are available in the Supporting Information. The C/N ratio of a single monomer unit and aminosilane is 7 and 3, respectively. Because the majority of the organic material is from the polymer, one would expect samples with more polymer to have C/N ratios close to 7 and those with greater influence from the silane to have slightly lower values. Elemental analysis and TGA calculations show this to be, in fact, the case. XPS similarly shows values very consistent with EA and TGA, though some numbers are slightly askew, probably due to residual carbon on the external surface or carbon tape used in the measurement. The C/Si ratios calculated from TGA match the EA very well.

Infrared Spectroscopy. Transmission FT-IR was used to verify the presence of the peptide brushes as manifested by the appearance of the amide I and II bands. Figure 3 shows the spectra obtained for the three initial amine loadings for the MCM-41 composites. The spectra for the SBA-15 and KIT-6 samples are in the Supporting Information. In all the samples—save the low amine loading composite for KIT-6—the benzyl carbamate (~1700 cm^{-1}), amide I (~1655 cm^{-1}), amide II (~1545 cm^{-1}, plus ~3080 cm^{-1} overtone), and amide A (~3300 cm^{-1}) bands

Table 2. Elemental Composition[a]

sample ID	C/N_{TGA}	C/N_{XPS}	C/N_{EA}	C/Si_{TGA} (wt %)	C/Si_{EA} (wt %)
PZK-0.75APTMS-MCM41	6.61	7.84	5.92	0.98	1.09
PZK-0.50APTMS-MCM41	6.82	6.88	5.91	1.02	1.05
PZK-0.25APTMS-MCM41	6.93	7.31	5.60	0.62	0.66
PZK-0.75APTMS-SBA15	6.70	6.72	6.52	1.33	1.40
PZK-0.50APTMS-SBA15	6.85	6.88	6.60	1.23	1.19
PZK-0.25APTMS-SBA15	6.92	8.09	6.36	0.60	0.67
PZK-0.75APTMS-KIT6	6.40	7.25	5.81	0.63	0.45
PZK-0.50APTMS-KIT6	6.33	7.50	5.30	0.26	0.24
PZK-0.25APTMS-KIT6	6.67	9.29	4.49	0.15	0.15

[a] "TGA" denotes theoretical values calculated from the TGA results; "XPS", from X-ray photoelectron spectroscopy; and "EA", from elemental analysis. C/N and C/Si ratios are on a molar and weight basis, respectively.

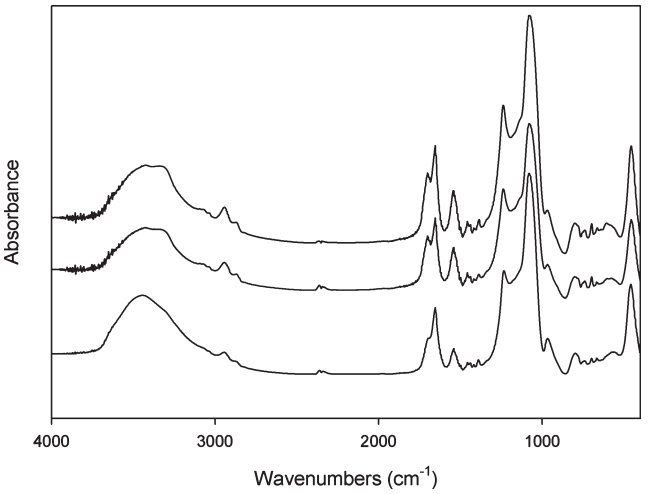

Figure 3. IR spectra of the Poly-Z-L-lysine−MCM-41 composites. From top to bottom 0.75, 0.50, and 0.25 mmol APTMS/g SiO_2.

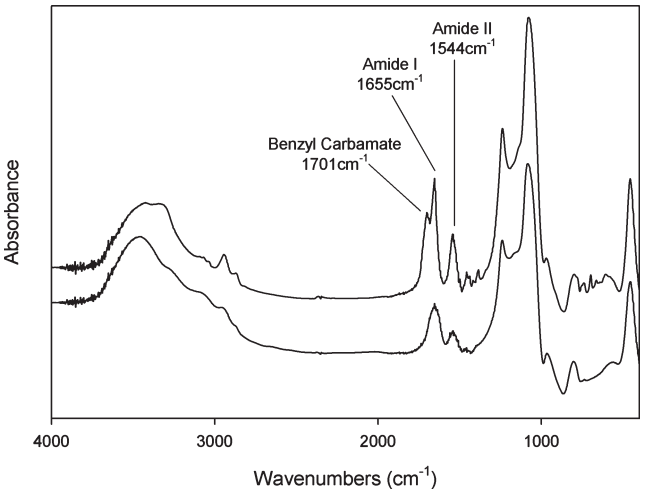

Figure 4. IR spectra of the protected (top) and deprotected (•HBr) (bottom) 0.75 mmol APTMS/g SiO_2 poly-Z-L-lysine−MCM-41 composite.

are clearly present. Additionally, bands resulting from C−H stretching in the lysine side chain and organosilane can be observed between 2800 cm^{-1} and 3000 cm^{-1}. The silanol (Si−OH) and Si−O−Si bands from the parent materials are likewise observed at ~3450 cm^{-1} (broad) and ~1080 cm^{-1}, respectively. The amide peaks are more intense relative to those corresponding to the parent material for the composites with higher initial amine loadings, indicating qualitatively higher peptide loadings for higher initial amine loadings, consistent with the TGA and porosimetry results. Accurate determination of peptide conformation based on the amide I and II bands alone is difficult due to the broadness of the peaks and water adsorption in the same region; more in-depth studies are needed.

Accessibility to the side-chain amine groups is important for many applications and motivated our efforts to successfully remove the Cbz protecting group. Figure 4 shows the IR spectra for the deprotected and protected 0.75 mmol APTMS/g MCM-41 composite. The absence of the benzyl carbamate peak and retention of the amide I and II peaks evidence effective deprotection of the side chain amines while avoiding amide hydrolysis. TGA on the resulting deprotected composites compares very well with our calculations. For example, the deprotected 0.25 mmol APTMS/g MCM-41 composite showed an organic content of 19.8 wt % compared to the calculated 18.6 wt %. While we cannot quantify the extent of deprotection by IR, the benzyl carbamate is essentially absent, and there is a dramatic decrease in the intensity of the C−H stretches in the range of 2800−3000 cm^{-1}. More evidence for effective deprotection is given by NMR.

$^{13}C\{^1H\}$ CP MAS NMR. Solid state NMR spectroscopy provides further evidence for peptide formation within the composite (Figure 5). $^{13}C\{^1H\}$ CP MAS NMR was performed on the protected and deprotected 0.75 mmol APTMS/g MCM-41 peptide−MCM-41 composite. The characteristic peaks due to the aliphatic lysine side chain carbons (α, β, γ, δ, and ε) are present in the spectra for both materials between 20 ppm and 60 ppm.[66] The amide carbon has a resonance of 173−175 ppm and is similarly present in both spectra. The peaks between 60 ppm and 170 ppm are the aromatic carbons, the benzylic carbon, and the carbamate carbon from the protecting group;[67] they are significantly diminished after treatment with HBr. Two of the aminosilane carbons are obscured by the resonances for the lysine side chain; however, the α-carbon peak (with reference to the silicon)

(66) Kricheldorf, H. R.; Muller, D. *Macromolecules* **1983**, *16*, 615–623.

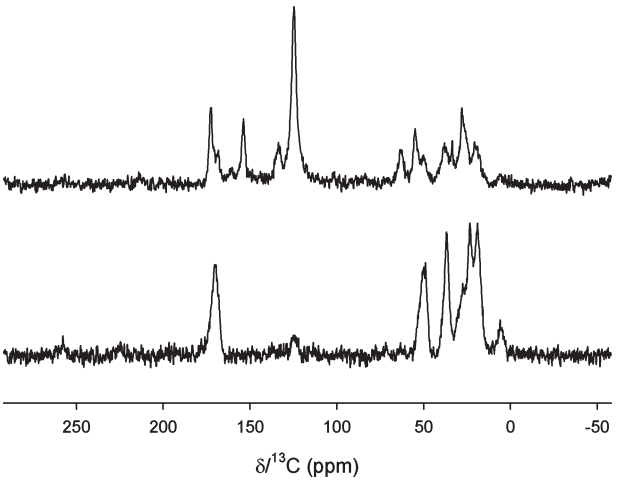

Figure 5. $^{13}C\{^{1}H\}$ CP MAS NMR of the side chain protected (top) and deprotected (•HBr) (bottom) 0.75 mmol APTMS/g MCM-41 poly-Z-L-lysine composite.

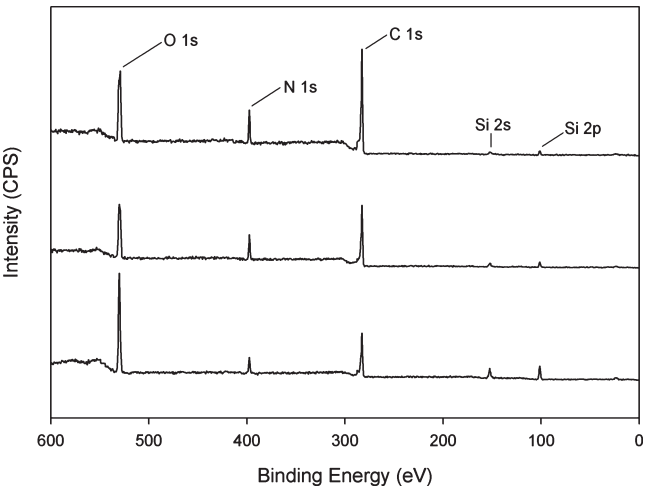

Figure 6. XPS of the poly-Z-L-lysine−MCM-41 composites: 0.75 mmol APTMS/g (top); 0.50 mmol APTMS/g (middle); and 0.25 mmol APTMS/g (bottom).

can be seen at approximately 7 ppm.[20] The presence of the amide carbon peak in the protected composite confirms the IR data demonstrating peptides are indeed formed in the composite. Similarly, the fact that this peak is preserved following deprotection provides additional evidence of the peptide structure being retained upon treatment with HBr. Another interesting feature is the lack of any carboxylic acid carbon peak at approximately 180 ppm. If peptide was formed in solution and merely adsorbed on the surface it seems likely this peak would be observed.

X-ray Photoelectron Spectroscopy. XPS was used to investigate the elemental composition of the composites' surfaces. Figure 6 shows the XPS spectra for the side-chain protected MCM-41 composites; the spectra for the SBA-15 and KIT-6 are included in the Supporting Information. The XPS results indicate significant amounts of organic on the outer surface as indicated by the large N 1s (405 eV) and C 1s (284 eV) peaks compared to the Si 2p (100 eV). The KIT-6 composites on the other hand appear to show little outer surface functionalization. This result corroborates the above IR, porosimetry, and TGA data above which show little peptide is grafted to the KIT-6 composites, especially at low loadings of amine initiator. Also, just as in the IR, we see evidence for increased organic on the surface with increased amine loadings for all three OMS materials. The C/N ratios vary between 6.7 and 8.1 (Table 2); this compares closely to the expected value of 7 (C/N ratio for Lys(Z) monomer unit). As noted above, variance on the upper end can most likely be attributed to residual carbon on the OMS surface prior to functionalization or the carbon tape used in the measurement; variance on the lower end can be attributed to the influence of the aminopropylsilane initiator. The only sample that deviates from the above range is the 0.25 mmol APTMS/g KIT-6 peptide composite, which has a C/N of 9.3. As the amount of organic on the surface is small compared to the others, the residual carbon has a much larger impact on the intensity of the C 1s peak. As additional evidence of peptide formation on the external surface, splitting can be seen in high resolution scans of the C 1s peak that occurs in the same manner as in poly-Z-L-lysine (Supporting Information).

Mass Spectrometry. MALDI-TOF MS has been shown in the literature to be quite useful in determining molecular weight distributions of low molecular weight homopolymers, especially when the distribution is narrow;[67−71] this approach has also been used for polypeptides.[72] Wanting to obtain a better understanding of the influence of pore size, topology, and initiator loading on the peptide molecular weights, MALDI-TOF MS was performed on peptide obtained from the three SBA-15 composites and the 0.5 mmol APTMS/g OMS initiator loading of the MCM-41 and KIT-6 composites by dissolution of the silica framework. Figures 7−9 show the MALDI-TOF MS spectra for the three PZK-SBA-15 composites. Observed chemical species include the protected peptide with fluorinated silane and the protected polymer with fluorinated silane that is missing one Z protecting group. The 0.25 mmol APTMS/g SiO_2 SBA-15 composite shows a rather normal distribution of molecular weights centered on peptide lengths of 4−6. The results for the higher initiator loadings in SBA-15 show a less well-defined distribution that is shifted slightly toward lower chain lengths of 3−4. The 0.5 mmol APTMS/g SiO_2 loading of the MCM-41 and KIT-6 composites closely resembles these two samples with distributions centered on chain lengths of 3−4 (Supporting Information). In the SBA-15 composites, the peptide length is limited to ∼9 monomer units. This limit is reasonable considering the pore size of SBA-15 is 8 nm, the length of one monomer unit

(67) Hanton, S. D. *Chem. Rev*. **2001**, *101*, 527–569.
(68) He, M. Y.; Chen, H. *Curr. Org. Chem*. **2007**, *11*, 909–923.
(69) Ji, H. N.; Nonidez, W. K.; Advincula, R. C.; Smith, G. D.; Kilbey, S. M.; Dadmun, M. D.; Mays, J. W. *Macromolecules* **2005**, *38*, 9950–9956.
(70) Ji, H. N.; Sakellariou, G.; Mays, J. W. *Macromolecules* **2007**, *40*, 3461–3467.
(71) Ji, H. N.; Sato, N.; Nonidez, W. K.; Mays, J. W. *Polymer* **2002**, *43*, 7119–7123.
(72) Lu, H.; Cheng, J. J. *J. Am. Chem. Soc*. **2008**, *130*, 12562–12563.

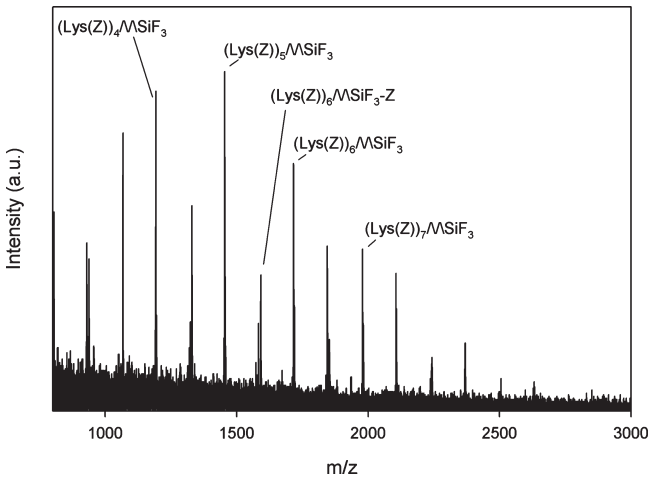

Figure 7. MALDI-TOF MS of peptide from the 0.25 mmol APTMS/g SBA-15 poly-Z-L-lysine composite. Note the spacing of peaks is equivalent to the mass difference of one monomer or the loss of a single Cbz protecting group. Only select peaks are labeled.

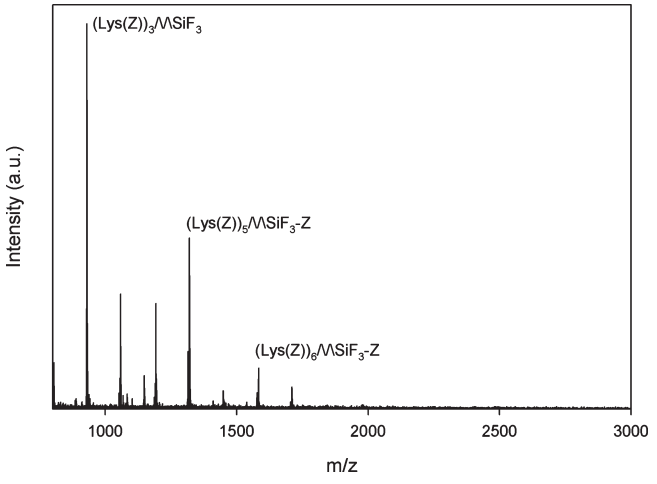

Figure 8. MALDI-TOF MS of peptide from the 0.50 mmol APTMS/g SBA-15 poly-Z-L-lysine composite. Note the spacing of peaks is equivalent to the mass difference of one monomer or the loss of a single Cbz protecting group. Only select peaks are labeled.

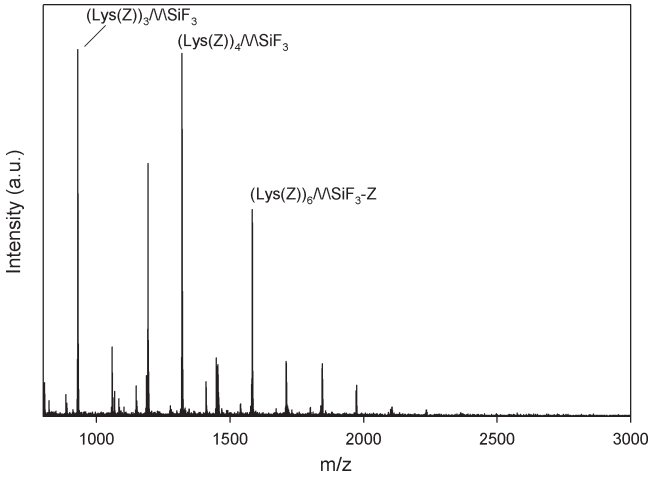

Figure 9. MALDI-TOF MS of peptide from the 0.75 mmol APTMS/g SBA-15 poly-Z-L-lysine composite. Note the spacing of peaks is equivalent to the mass difference of one monomer or the loss of a single Cbz protecting group. Only select peaks are labeled.

is about 3.5 Å when elongated, and the rather large side chain of L-Lys(Z).

Catalytic Data (*Henry Reaction*). To look at the accessibility of the side chain amines in the deprotected L-lysine composites, the nitroaldol (Henry) reaction between *p*-nitrobenzaldehyde and nitromethane was used as a probe. Catalytic testing was performed on the low initiator loading for MCM-41 and SBA-15 and the high initiator loading for all three OMS materials. These results are tabulated in Table 3. Conversions match closely with the with the porosimetry data, showing that higher conversions and turnover frequencies (TOF) are obtained for samples with higher porosity. The selectivity between the alcohol (A) and unsaturated product (B) is fairly constant in all samples where conversion was observed.

Poly-L-alanine (PA)−OMS Composites. Composites were also synthesized using L-alanine NCA to contrast with the much larger L-lysine(Z) monomer. All three amine loadings were synthesized on SBA-15, while only the 0.5 mmol APTMS/g SiO_2 was synthesized on MCM-41 and KIT-6. The same battery of characterization techniques was employed to analyze these samples.

N_2 Adsorption. Nitrogen porosimetry shows a similar trend to the poly-Z-L-lysine composites in that there is decreasing porosity with increased initial amine loading. The lowest loading still maintains about half of its initial porosity, the mid-loading with significantly less, and the high loading with essentially no porosity. The pore diameter also incrementally decreases with increasing initiator loading, akin to the KIT-6 composites of PZK. In the MCM-41 and KIT-6 composites, similar pore volumes, and surface area decreases to the SBA-15 composites occur; however, BJH analysis indicates the pore diameters are much smaller. This makes sense for MCM-41, as its pore diameter is much smaller prior to any functionalization. The much more dramatic decrease in the KIT-6 pore diameter is probably due to its lower initial pore volume.

Thermogravimetric Analysis. TGA on the three poly-L-alanine composites on SBA-15 showed weight losses of 42.42 wt %, 40.19 wt %, and 41.15 wt % for the 0.75, 0.50, and 0.25 mmol APTMS/g SBA-15 composites, respectively. For the MCM-41 and KIT-6 composites, similar results were obtained: 40.03 wt % and 36.59 wt %, respectively. This weight loss corresponds to a complete or near complete polymerization (i.e., 100% monomer conversion). This result is interesting in that porosity changes in the poly-Z-L-lysine composites were associated also with a difference in overall organic content; in contrast, here all three samples have essentially the same organic content by TGA. We speculate that this is a result of increased spacing of more or less equal length polymers inside the pores at low initial amine loadings with polymers of increased length on the external surface. This result indicates that porosity in the poly-L-alanine composites can be controlled purely by the surface initiator loading. It is also noteworthy that the high organic content and low porosity of the KIT-6 composite contrast significantly with those in PZK KIT-6

Table 3. Catalytic Results for the Nitroaldol Reaction between *p*-Nitrobenzaldehyde and Nitromethane

	MCM-41			SBA-15			KIT-6		
mmol APTMS/g SiO_2	X (7 h)	A/B	TOF (h^{-1})	X (7 h)	A/B	TOF (h^{-1})	X (7 h)	A/B	TOF (h^{-1})
0.25	40%	1.1	5.7	37%	0.8	5.3			
0.50									
0.75	2%	0.8	0.3	~0	N/A	N/A	16%	1.3	2.3

Table 4. Tabulated Nitrogen Adsorption Results for the Poly-L-alanine−OMS Composites

sample	$S(\alpha_s)$ [m^2/g]	V_{meso} [cm^3/g]	d_p(BJH) [nm]
MCM-41	1084	0.71	2.8
PA-0.50APTMS-MCM-41	360	0.13	< 1.5
SBA-15	918	0.93	7.0
PA-0.25APTMS-SBA15	662	0.39	5.6
PA-0.50APTMS-SBA15	233	0.10	4.8
PA-0.75APTMS-SBA15	143	0.05	< 1.5
KIT-6	1091	0.59	7.6
PA-0.50APTMS-KIT6	268	0.12	< 1.5

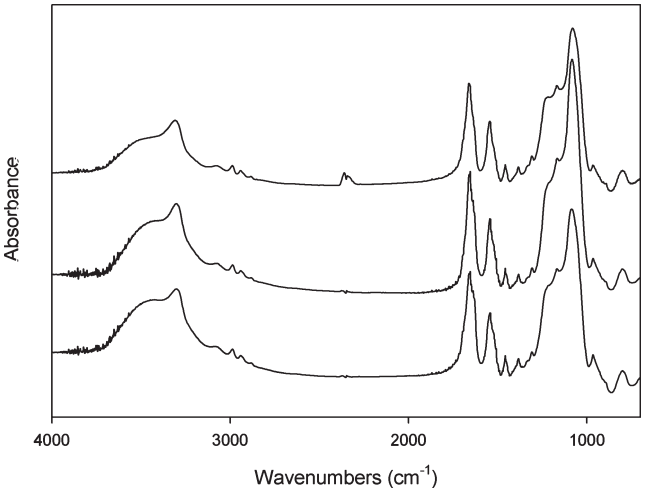

Figure 10. IR spectra of the poly-L-alanine−SBA-15 composites: 0.75 mmol APTMS/g (top); 0.50 mmol APTMS/g (middle); and 0.25 mmol APTMS/g (bottom).

composites which showed little peptide functionalization.

Infrared Spectroscopy and X-ray Photoelectron Spectroscopy. FT-IR spectra as in the poly-Z-L-lysine composites confirm the presence of poly-L-alanine. The amide I and II bands can be seen at about 1660 cm^{-1} and 1545 cm^{-1}, respectively (Figures 10 and 11). The amide A (3310 cm^{-1}) and C−H stretches (2800−3000 cm^{-1}) are also clearly observed. It is noteworthy that the intensities of the amide bands (I, II ,and A) are stronger relative to the silanol and Si−O−Si bands than in the PZK composites. This result is very reasonable when we take into account the high organic loadings (observed by TGA) and the much smaller side chain of alanine (compared to PZK). XPS analysis of the surface likewise shows a very large amount of polymer on the surface, as evidenced by the domination of the spectra by the N 1s and C 1s peaks; the Si 2s and 2p peaks are almost nonexistent (Figure 12).

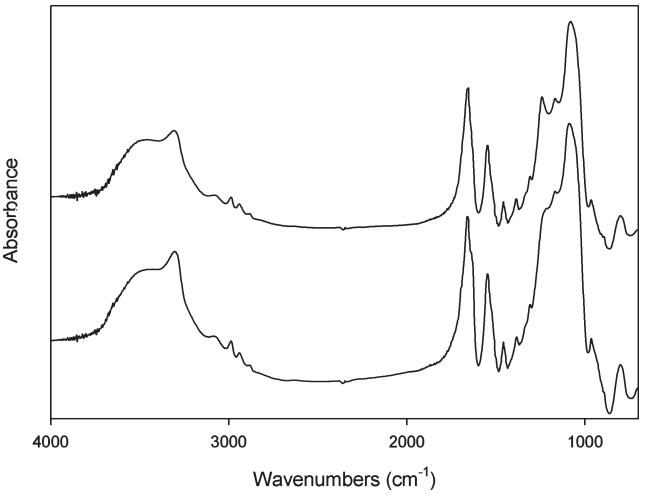

Figure 11. IR spectra of the poly-L-alanine−MCM-41 (top) and KIT-6 (bottom) composites, both containing 0.5 mmol ATPMS/g SiO_2.

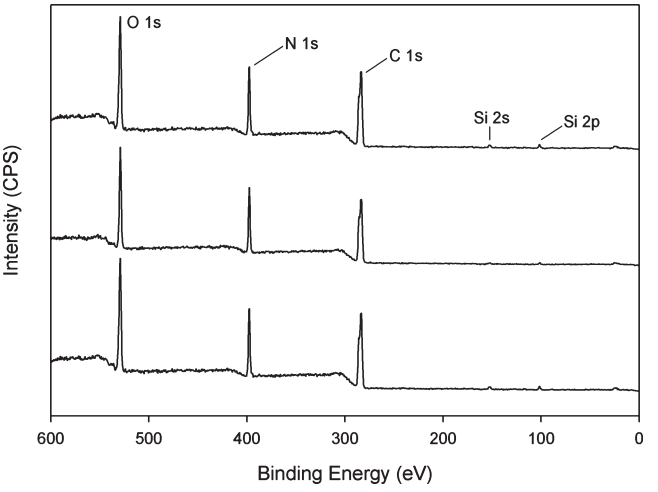

Figure 12. XPS of the poly-L-alanine−SBA-15 composites: 0.75 mmol APTMS/g (top); 0.50 mmol APTMS/g (middle); and 0.25 mmol APTMS/g (bottom).

Mass Spectrometry. MALDI-TOF MS was also performed on the poly-L-alanine−OMS composites. Results show polymers of much longer chain lengths than in the PZK composites with an upper bound of about 35-mer units in the SBA-15 composites. Observed chemical species include the peptide with fluorinated silane and the peptide without the silane. Figures 13−15 show the MALDI-TOF MS results for the poly-L-alanine−SBA-15 composites. In the low initiator loading of the SBA-15 composites, as in the PZK−SBA-15 composite, the molecular weight distribution looks almost Gaussian and is centered on chain lengths of 24 and 25. There is also a large peak corresponding to the 12 monomer unit. At the higher initiator loadings, the molecular

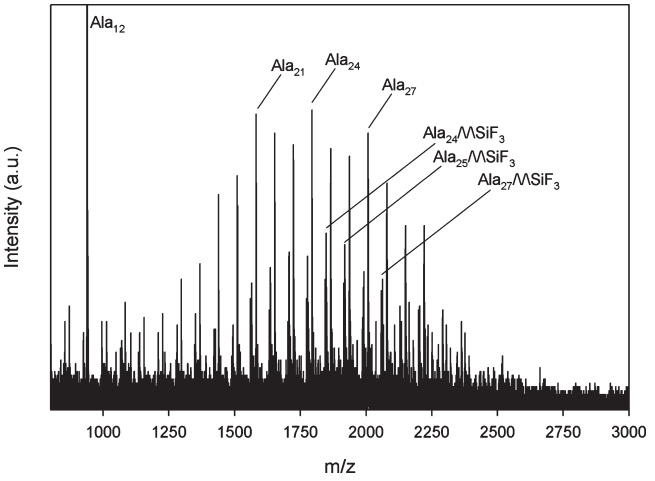

Figure 13. MALDI-TOF MS of peptide from the 0.25 mmol APTMS/g SBA-15 poly-L-alanine composite. Note the spacing of peaks is equivalent to the mass difference of one monomer. Only selected peaks are labeled.

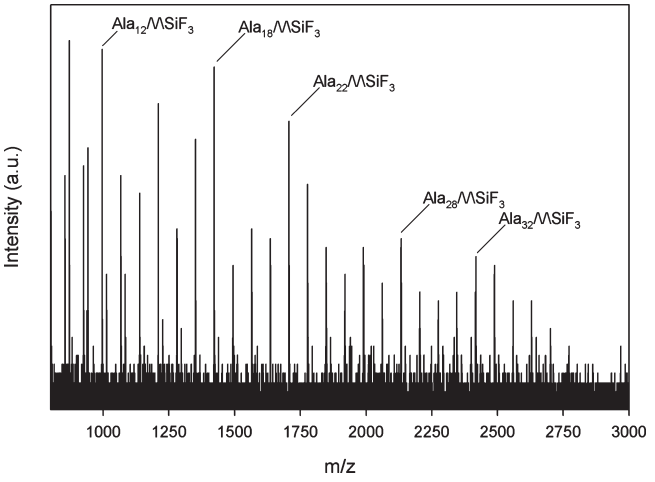

Figure 14. MALDI-TOF MS of peptide from the 0.50 mmol APTMS/g SBA-15 poly-L-alanine composite. Note the spacing of peaks is equivalent to the mass difference of one monomer. Only select peaks are labeled.

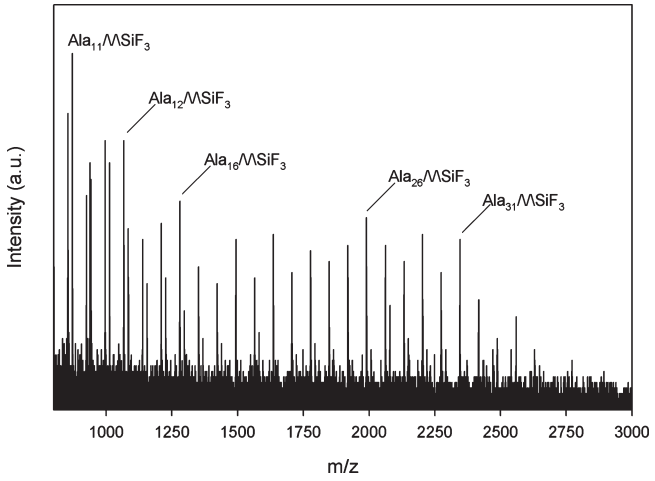

Figure 15. MALDI-TOF MS of peptide from the 0.75 mmol APTMS/g SBA-15 poly-L-alanine composite. Note the spacing of peaks is equivalent to the mass difference of one monomer. Only select peaks are labeled.

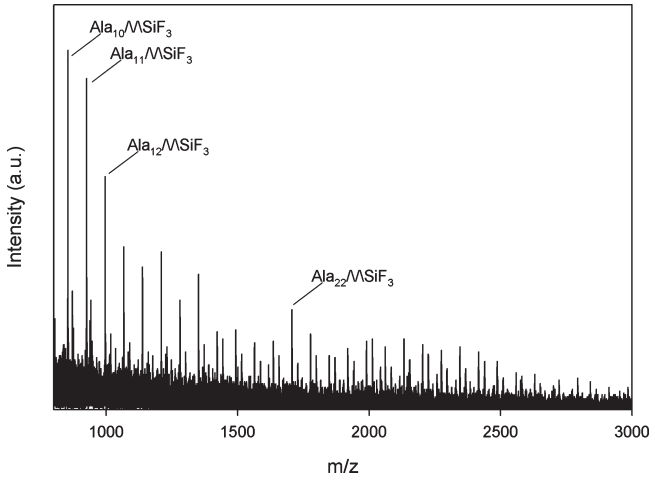

Figure 16. MALDI-TOF MS of peptide from the 0.50 mmol APTMS/g MCM-41 poly-L-alanine composite. Note the spacing of peaks is equivalent to the mass difference of one monomer. Only select peaks are labeled.

weight distributions become broader and almost bimodal at the highest loading. This phenomenon makes sense when we take into consideration the monomer to initiator ratio at the higher loadings is 20 and 13, lower than the average chain length observed for the low initiator loading composite. The MALDI-TOF MS results for the MCM-41 composite show a much smaller molecular weight with a prevalence of much smaller chains (Figure 16). This result demonstrates the confining effect the pore size has on peptide growth. Interestingly, this effect was not noticeable in the PZK composites. In the KIT-6 composite, the molecular weight distribution is shifted to the left of the corresponding SBA-15 sample, though not as dramatically as in MCM-41 (Figure 17).

Discussion

Effect of Initial Amine Loading. The overall influence of the initial amine loading is on the porosity of the samples primarily. In the PZK composites, there is a notable change in the overall organic content with changing amine loadings, but this is probably more a result of the bulky monomer and difficulty reaching high molecular weights than strictly on amine loading. In the PA samples, which show no content differences by TGA, the effect of the amine loading can be seen more clearly. In these samples, as in the PZK composites, the porosity increases with decreasing amine loading. The authors believe this has to do with the increase in spacing of polymers with equal or similar lengths inside the pores, with longer polymers on the external surface for the low initiator loadings to make up for the difference in weight. Our mass spectrometry results, which show similar results for various amine loadings in the same OMS material, are evidence of this conclusion.

Effect of Pore Size (MCM-41 vs SBA-15). In the PZK composites, the pore size seems to have little effect in terms of the molecular weight of the polymer obtained by MALDI-TOF MS. In terms of the amount of organic in the pores, SBA-15 was able to accommodate more organic, likely due to its higher pore volume. In the PA composites, we see a clear difference in the molecular weight of the polymer between SBA-15 and MCM-41:

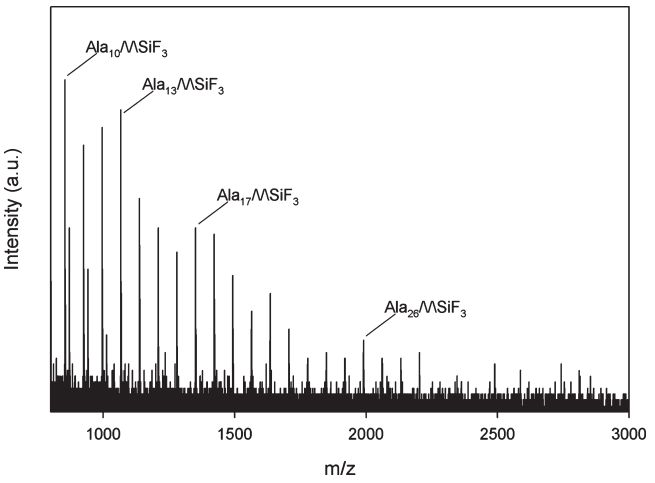

Figure 17. MALDI-TOF MS of peptide from the 0.75 mmol APTMS/g KIT-6 poly-L-alanine composite. Only select peaks are labeled.

SBA-15 affords longer polymers and MCM-41 shorter polymers. A simple way to interpret this result is that the OMS mesopores provide confinement effects that influence the final polymer molecular weight.

Effect of Pore Topology (SBA-15 vs KIT-6). The effect of the pore topology is fairly dramatic, especially in the case of the PZK composites: the organic contents in the PZK composites of KIT-6 are very low, and the porosities are quite high compared with those on SBA-15. In the case of PA, the organic contents and porosity are almost the same for the 0.5 mmol APTMS/g SiO_2 composites of SBA-15 and KIT-6. We do, however, see smaller molecular weights in the MALDI-TOF MS for the PA KIT-6 composite synthesized. Though the exact reason for the differences between peptide growth on KIT-6 and SBA-15 and between PZK and PA on KIT-6 remains unclear, it is likely that it is related to topological differences as KIT-6 and SBA-15 have roughly the same pore diameter and surface area. Some factors that may play roles include: pore dimensionality (2D vs 3D), local/overall pore curvature, and local/overall surface silanol densities.

Effect of Monomer Identity (L-Lys(Z) NCA vs L-Ala NCA). As evident from the TGA and MALDI-TOF showing the accommodation of much longer chains in the pores, PA packs significantly better than the PZK because of its substantially smaller side chain. The longer peptide chains may also be attributed to folding of the polymer. Another notable difference between the two systems is that the PA composites maintain some porosity at high organic loadings while the PZK composites do not.

Conclusions

The results show that NCA polymerization chemistry can be used to synthesize well-defined composite materials with ordered mesoporous silica. The properties of the composite and the attached polymer can be tuned by altering the surface initiator loading, pore size, pore topology, and monomer identity. For the poly-Z-L-lysine composites, it has been demonstrated that the polymer can be deprotected to yield the active side chain amine without deterioration of the polymer. This result also evidences the accessibility of the side chain groups despite the high organic loadings and the lack of porosity by nitrogen adsorption. In addition, the presented catalytic data of the deprotected composites demonstrates accessibility to larger molecules for composites with slightly more porosity. For the poly-L-alanine−SBA-15 composites, the porosity can be tuned by changing the initiator loading while having no ill effect on overall organic content and minimal effect on the polymer molecular weight obtained.

Acknowledgment. This work was supported financially by the Robert A. Welch Foundation (Grant A-1638). Additionally, the authors would like to acknowledge the Materials Characterization Facility at Texas A&M for use of their Kratos Axis Ultra Imaging X-ray photoelectron spectrometer and the Chemistry Department for access to their X-ray diffraction facilities and the Laboratory for Biological Mass Spectrometry. The authors would also like to thank Qingqing Wang for the solid state NMR measurements.

Supporting Information Available: IR and XPS spectra for the PZK composites of SBA-15 and KIT-6, including the high resolution C 1s XPS scan for the 0.75 mmol/g MCM-41; MALDI-TOF results for the 0.5 mmol APTMS/g SiO_2 PZK composites of MCM-41 and KIT-6; and complete tabulated TGA and EA results. This material is available free of charge via the Internet at http://pubs.acs.org.